1-1-1985

Response of Lithographic Mask Structures to Repetitively Pulsed X-rays: Thermal Stress Analysis

A. Ballantyne
Avco Everett Reserach Labortory, Inc.

H.A. Hyman
Avco Everett Reserach Labortory, Inc.

Clive L. Dym
Harvey Mudd College

R.C. Southworth
Avco Systems Division

AIP | Journal of Applied Physics

Response of lithographic mask structures of intense repetitively pulsed x rays: Thermal stress analysis

A. Ballantyne, H. Hyman, C. L. Dym, and R. Southworth

Citation: Journal of Applied Physics **58**, 4717 (1985); doi: 10.1063/1.336245
View online: http://dx.doi.org/10.1063/1.336245
View Table of Contents: http://scitation.aip.org/content/aip/journal/jap/58/12?ver=pdfcov
Published by the AIP Publishing

Response of lithographic mask structures of intense repetitively pulsed x rays: Thermal stress analysis

A. Ballantyne and H. Hyman
Avco Everett Research Laboratory, 2385 Revere Beach Parkway, Everett, Massachusetts 02149

C. L. Dym
University of Massachusetts, Amherst, Department of Civil Engineering, Amherst, Massachusetts 01003

R. Southworth
Avco Systems Division, 201 Lowell Street, Wilmington, Massachusetts 01887

(Received 22 October 1984; accepted for publication 27 March 1985)

This paper examines the effects of thermal loading and time history upon the thermal stresses developed in lithographic mask structures as would be expected under irradiation by intense soft x rays. The objective of this work was to examine the phenomenology of the interaction and to evaluate the limits placed upon mask dosage. The mechanics of mask failure are examined in terms of single pulse and cumulative, or fatigue, effects. A number of prototypical mask structures are investigated, which show that the application of intense pulsed sources to x-ray lithography does not reduce the potential utility of the techique. However, it is shown that the estimated damage thresholds do impact the operating conditions chosen for optimal production rates and mask lifetime.

I. INTRODUCTION

There has recently been a growing interest in intense pulsed plasma sources suitable for high-resolution microlithography applications.[1,2] A common characteristic of all such plasma sources is that each intense x-ray pulse is of very short time duration, typically ~ 1–100 nsec. Thermal energy is thus deposited very rapidly into the x-ray mask structure, and since the heat cannot be dissipated in such a short time, the potential exists for damaging the mask. We have therefore carried out an extensive theoretical analysis to investigate the response of lithographic mask structures to intense, repetitively pulsed irradiation.

The first of this series of papers[3] summarized the important mask damage mechanisms and related them to key x-ray lithography system parameters (e.g., throughput, resolution). The potential damage effects were found to fall into two broad categories: (1) the development of large thermal stresses at the absorber/substrate interface due to rapid heating, and (2) the dynamic response under repetitively pulsed loading. Although an overview of the thermal stress problem was given in Ref. 3, no attempt was made to present the complete and detailed analysis. The purpose of the present paper is to develop the theoretical model and apply it to a detailed analysis of thermal stress-induced mask damage effects. The final paper of the series[4] will consider the dynamic response of the mask structure.

The following sections examine the effects of thermal loading and time history upon the thermal stress levels generated in the mask. These are particularly severe for the region near the interface between substrate and the x-ray absorbing lithographic pattern bonded to it. A substantial fraction of the incident radiation is absorbed in the mask and large temperatures can occur on short timescales. Interpulse cooling plays a significant role in the thermal stress time history.[3] The stress field has been modeled both analytically and by finite difference codes, and has been examined in the light of potential single-pulse failure and multipulse fatigue damage limits upon iradiation dosages.

Many types of mask structure have been fabricated. Table I includes but a (representative) sample of the wide variety of substrate and sandwich material types that have been used. These have, for the most part, only been used under cw irradiation.

The objectives of this work were to examine the phenomenology of the mask radiation interaction and to evaluate the limits placed upon mask dosage for a variety of prototypical mask structures. These include the use of gold absorber upon silicon, beryllium, and polymeric materials, as well as examining the effect of interface materials that promote improved bonding between the absorber and substrate.

II. MASK THERMAL LOADING

A. Mask thermal loading

The mask is subject to a repetitively pulsed x-ray loading. We are typically considering mask thickness of order of $5\ \mu$m. A significant fraction of the x-ray fluence incident on the mask is absorbed in the substrate, and most of that incident on the absorber layer is absorbed. For an instantaneous deposition, the temperature rise at the absorber-substrate interface is given by

$$\Delta T_{\max} = \frac{J_0}{(\rho c)_a \lambda_a}, \tag{1}$$

where J_0 is the fluence delivered to the resist. (This is, of course, substantially smaller than is incident in the substrate.) However, the actual temperature rise in the mask is governed by conduction. The temperature history in the mask is governed by the classical heat conduction equation, but modified by an in-depth energy absorption, viz.,

$$\frac{\partial \Theta}{\partial t} = \alpha_{\text{th}} \frac{\partial^2 \Theta}{\partial x^2} + \frac{\phi e^{-x/\lambda}}{(\rho c)\lambda}, \tag{2}$$

 0021-8979/85/244717-09$02.40

TABLE I. X-ray lithography mask structures.

Subtrate	Reference
Silicon	D. L. Spears and H. I. Smith (see Ref. 5)
Silicon carbide	R. K. Watts, K. E. Bean, and T. L. Brewer (see Ref. 6)
Silicon nitride	E. Basseous, R. Feder, E. Spiller, and E. Toplain (see Ref. 7)
Alumina	P. A. Sullivan and J. H. McCoy (see Ref. 8)
Polyimide	P. Parrens, E. Tabouset, and M. C. Tacussel (see Ref. 9)
Mylar	D. Maydan, G. A. Coquin, J. R. Maldonado, S. Somek, D. Y. Lou, and G. E. Taylor (see Ref. 10)
Beryllium	D. J. Nagel, M. C. Pekerar, R. R. Whittock, J. R. Grieg, and R. E. Pechacek (see Ref. 11)
Boron nitride/polyimide	D. Maydan, G. A. Coquin, H. J. Levinstein, A. K. Sinha, and D. N. K. Wang (see Ref. 12)
$Si_3N_4/SiO_2/Si_3N_4$	T. Hayashi (see Ref. 13)
$Si_3N_4/Si_xO_yN_z/Si_3N_4$	L. Csepregi and A. J. Heuberger (see Ref. 15)

where ϕ is the incident flux density. Beer's Law of absorption of x-ray energy is valid for the soft x rays used in x-ray lithography as scattering is insignificant. If we consider a mask with uniform thermal properties and comprising an absorber upon a perfectly transmitting substrate, a useful analytic approximation is available if we consider the substrate to be semi-infinite in extent. This is valid for the short pulse lengths generated by pulsed laser sources. Solving Eq. (2) by standard Laplace transform techniques,[16] we obtain a value for the temperature rise at the interface given by

$$\Theta_{\text{interface}} = \Delta T_{\max}\left\{\left(\frac{e^{\beta}-1}{\beta}\right)-\frac{e^{\beta}}{2\beta}\left[\operatorname{erfc}(-\sqrt{\beta})+\frac{1}{\epsilon^2}\operatorname{erfc}(2\gamma-\sqrt{\beta})-\operatorname{erfc}(\gamma-\sqrt{\beta})+\operatorname{erfc}(\gamma+\beta)\right]+\frac{h_a}{\lambda\epsilon\beta}\operatorname{erfc}(\gamma)-\frac{1}{2\beta}\left[\left(\frac{2h}{\lambda}-1\right)\operatorname{erfc}(2\beta)-1\right]+\frac{1}{\sqrt{\beta\pi}}\left(1+e^{-4\gamma^2}-\frac{2}{\epsilon}e^{-\gamma^2}\right)\right\}, \quad (3)$$

where

$$\beta = \alpha_{\text{th}}\,\tau_p/\lambda^2,$$

$$\gamma = h_a/(2\sqrt{\alpha_{\text{th}}\tau_p}),$$

and $\epsilon = \exp(h/\lambda)$ is the contrast ratio between incident and transmitted x-ray intensities, τ_p is the x-ray pulse duration, α_{th} is the thermal diffusivity, and h_a is the absorber thickness.

Figure 1 illustrates the temperature rise normalized to $\Delta T_{\max}$ for a range of operating conditions representative of pulsed sources. As can be seen, the effect of increased pulse duration is to reduce the magnitude of the temperature rise. For a pulse duration of ~2 ns and a wavelength of 10 Å, we obtain a maximum temperature of $\sim 0.2\Delta T_{\max}$. At 10 ns this is reduced to $0.1\,T_{\max}$.

A more accurate numerical prediction has been made for an actual mask configuration.[3] This shows that for a mask irradiated, conventionally, from the substrate direction, the temperature in the absorber layer is essentially uniform for the pulse duration in question, and corresponds reasonably well to the analytic approximation. The temperature in the substrate is governed by the exponential deposition profile through most of its thickness. The conduction depth from the interface is less than 1 μm for the pulse durations of interest.

Inversion of the x-ray irradiation direction leads to a significant change in temperature profile. The peak temperature in the gold is approximately 50% higher than for conventional irradiation and the substrate temperatures are significantly lower. (The comparison is for equal delivered fluence at the resist.)

The large temperature gradient across the interface region can be expected to contribute to the generation of thermal stress. The time scale for equilibration of temperature across the mask is of order $\sim h_a^2/\alpha$, which is in the range 10^{-7}–10^{-6} sec.

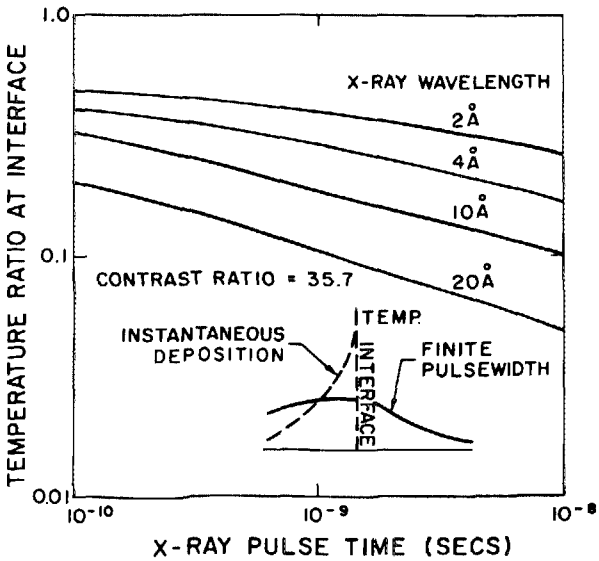

FIG. 1. Analytical model of ratio of conductively cooled interface temperatures to instantaneous deposition at typical x-ray pulse durations.

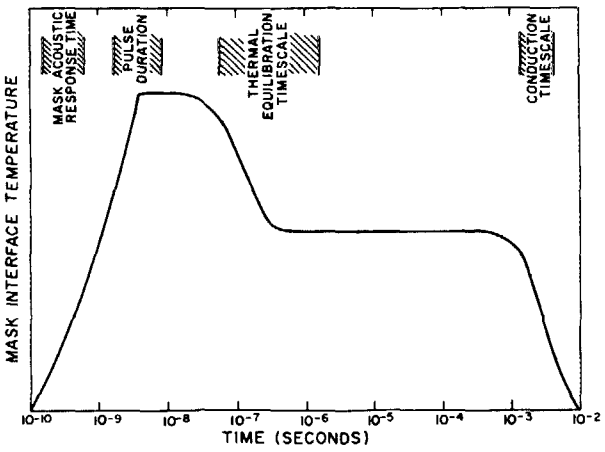

FIG. 2. Mask thermal history.

B. Mask cooling

As discussed in Ref. 3, the close proximity between the mask and wafer provides a very fast conductive cooling mechanism (see also Ref. 16). For source repetition rates of practical interest (i.e., <100 Hz), the absorbed energy in each pulse is essentially removed prior to the arrival of a subsequent pulse. The conductive cooling by the helium gas between wafer and mask is typically of order 10^{-3} sec. The thermal loading problem can therefore be treated on a single pulse basis. The cooling timescale by conduction is given by

$$\tau_{cond} = \frac{\rho c h l}{k_a} .$$

C. Mask time scales

Figure 2 illustrates the thermal history of the mask, in particular that of the absorber-substrate interface. The shortest time scale is that of the acoustic response time of the mask given by

$$\tau_{\text{acoustic}} = h / C_L ,$$

where h is the mask thickness and C_L is the longitudinal wave speed in the mask materials (~ 2200 m/s in gold, ~ 7000 m/s in silicon). This leads to acoustic times substantially shorter than the pulse time duration, which allows us to make the assumption that the stress behavior of the mask can be treated by classical static stress techniques. Subsequent to the pulse the temperature relaxes to its equilibrated value and then finally decays prior to further irradiation. The amount of energy stored in the mask when the next pulse arrives is given by

$$T_{\text{mask}} = \Delta T_0 \, e^{-t_p/\tau_{\text{cond}}} , \tag{5}$$

where $t_p/\tau_{\text{cond}} > 1$. For a 30-Hz repetition frequency this corresponds to $\sim 10^{-4} \Delta T_0$.

The steady-state temperature of the mask, for long pulse trains, is thus given by

$$T_{\text{mask}_{ss}} = J_0 \tau_{\text{cond}} R \frac{[(e^{h_s/\lambda_s} - 1) + \gamma(1 - e^{-h_a/\lambda_a})]}{[(\rho c h)_s + \gamma(\rho c h)_a]} , \tag{6}$$

where R is the repetition frequency and γ is the fractional area coverage by absorber. For a 10-mJ/cm^2 dosage, and 30-Hz operation this yields a temperature rise of ~ 1.0 K. For short duration runs, the temperature rise is approximately

$$T_{\text{mask}} \cong N \Delta T_0 \, e^{-t_p/\tau_{\text{cond}}} , \tag{7}$$

where N is the number of pulses delivered ($= t/R$). Thus, delivery of 100 pulses at 30 Hz yields a temperature rise $\sim 5 \times 10^{-7}$ K.

III. THERMAL STRESS MODELING

A. Damage mechanisms

The heating of the mask structure can lead to generation of thermal stress and strain. In particular, damage can occur at the interface region between substrate and absorber. This occurs as a consequence of different thermal expansion coefficients. The most likely form of damage is the delamination of the absorber from the substrate as a result of the induced shear stress at the interface between them. In addition, a large stress can be induced in the substrate in the vicinity of the edges of the absorbing elements (Fig. 3).

The stresses generated will be a function of the thermal deposition. The maximum stress will occur at termination of the x-ray pulse, and will also remain significant after thermal equilibration.

The baseline case study for this work is a gold/silicon mask structure. Other mask structures are considered in the next section. The properties of mask materials are given in Table II. Estimates of stresses and the damage criteria are made in order to assess the upper bound upon pulsed x-ray fluence that can be used without generating damage to the mask.

B. Stress modeling

A twofold approach was taken to modeling the stress field in the mask. An analytic approach was taken in order to scope the problem, providing physical insight into the magnitude of the stresses. A computer modeling effort was also undertakn to obtain a more detailed evaluation of the stress field.

1. Analytic stress model

A detailed derivation of the stress model can be found in Appendix A. The model has several assumptions: (1) The stress field is two dimensional. (2) There is a uniform temperature rise in the absorber. (3) The substrate is rigid and unheated.

The uniform temperature assumption is very reasonable in view of the temperature profiles obtained in the previous section. The rigid substrate is a good approximation for a high modulus material such as silicon, but will nontheless lead to some of overestimation of the stresses. This is because

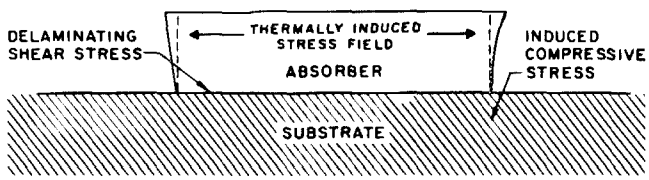

FIG. 3. Interface stress issues.

TABLE II. Mask properties.

	Young's modulus (psi×10⁷)	Expansion coefficient (×10⁻⁶)	Absorption coefficient[a] (μm⁻¹)	Density (g/cm³)	Specific heat (J/g K)
Gold	1.08	14.2	0.14	19.32	0.129
Silicon	1.55	2.3	5.0	2.33	0.75

[a] At 10-Å wavelength.

there is no strain relaxation occurring in the absorber, resulting from the imposed prevention of induced strain near the substrate surface. The shear stress developed in the interface is given by

$$\tau_{xz}(x,0) = \frac{14.28\, E\alpha\Delta T}{1+1.2\,\phi_r}\,\frac{\sinh(kL/2)\sinh(kx)}{[kL+\sinh(kL)]}, \tag{8}$$

$$\phi_r = \frac{\sinh(kL)-kL}{\sinh(kL)+kL},$$

$$k = \sqrt{\frac{1-2\nu}{2(1-\nu)}}\,(\pi/2h).$$

The numerical constants are for gold ($\nu = 0.42$). The variation of maximum stress with absorber dimension (L/h) is shown in Fig. 4. As can be seen, the shear stress tends to an asymptote at large L/h values. This is an important observation as it bounds the magnitude of expected shear stress for any given mask pattern feature size. The asymptotic shear stress is thus

$$\tau_{xz}(L/2,0) = 3.25\, E\alpha\Delta T. \tag{9}$$

The axial compressive stress is given by

$$\sigma_{xx}(x,0) \simeq -\frac{E\alpha\Delta T}{1-\nu} \simeq -1.7\, E\alpha\Delta T. \tag{10}$$

Thus for $L/h > 2$, the shear stress dominates at the interface.

2. Computer modeling of stress field

An existing generalized two-dimensional (or axisymmetric) structural analysis code[17] was used for this analysis. Two regimes of interest have been investigated with the code; the preceding analytic formulation has been modeled, using the rigid substrate assumption and a uniform absorber temperature, and more realistic temperature profiles and correct material characteristics have been used, in order to obtain more representative stress behavior.

The comparison of shear stress levels in the rigid substrate case can be seen in Fig. 4. They are in remarkably good agreement with the model. The axial variation of stress levels is shown in Fig. 5. The axial stress shows an axial variation with significantly higher stresses at the end of the block. The magnitudes of both stress components are not too dissimilar, although the computer results are higher than those of the analytic formulation. The stresses, both axial and shear, drop rapidly to zero at the free edge of the block, as one moves away from the interface. It is the corner point, between free edge and substrate surface that has the highest stress levels, and it is here that failure would be anticipated to occur in the form of a delamination arising out of shear loading. The stress levels indicated in Fig. 5 result from a 78 K temperature rise. This represents the average temperature of the gold absorber if all the energy absorbed remains in the gold for a resist dosage (J_0) of 10 mJ/cm². In fact, the conduction of heat into the silicon substrate will significantly reduce this. Reference to Fig. 2 indicates that a 2-ns pulse yields an effective average temperature of 53 K and a 10-ns pulse gives a 46 K temperature rise. These are 32% and 41% reductions in temperature for a given dosage. When comparing these and later results, care must be taken with definition of the relationship between dosage of x rays and temperature.

A series of runs were made with the code for gold/silicon masks with the temperature profiles as described earlier for large values of L/h. Figure 6 shows the axial stress contours in the region of the gold/silicon interface for a resist dosage of 10 mJ/cm², a temperature profile corresponding

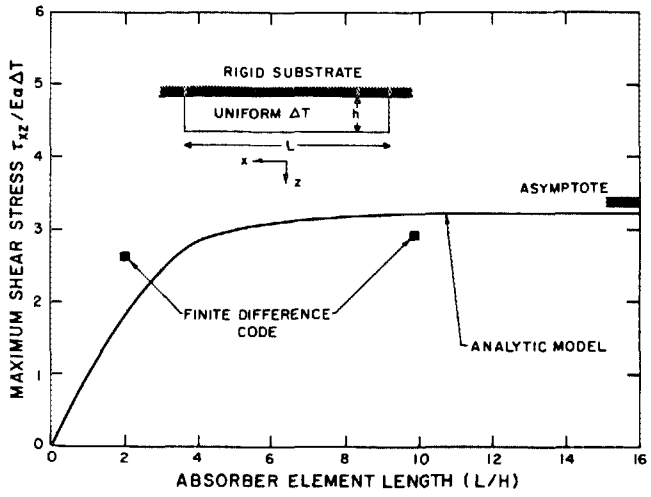

FIG. 4. Maximum shear stress at absorber/substrate interface as a function of element dimensions.

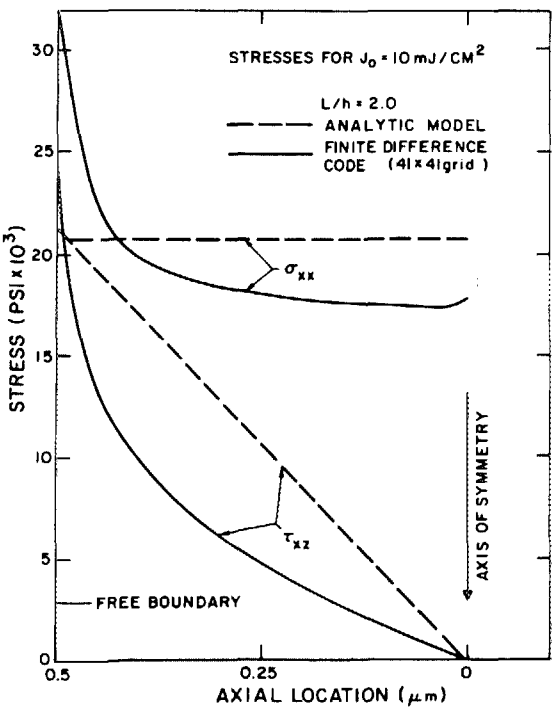

FIG. 5. Stress profiles along element length at substrate absorber interface.

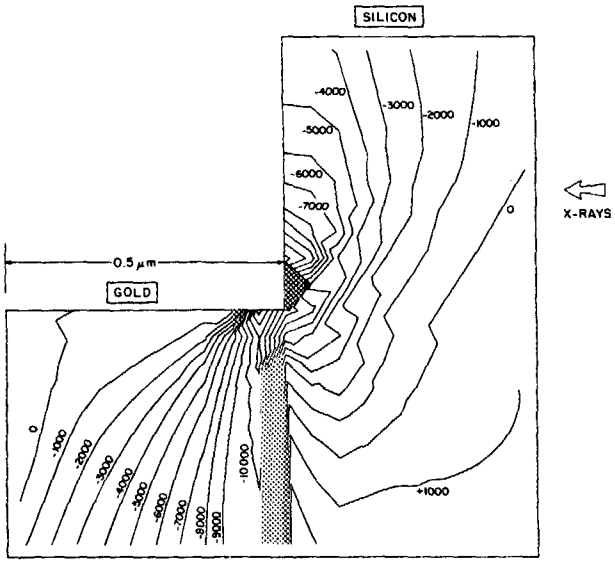

FIG. 6. Axial stress profiles near gold/silicon interface generated at x-ray pulse termination.

to an irradiation time of 2 ns, with $L/h = 10$. As can be seen, significant compressive stresses are generated near the absorber block end, within the substrate. The stress levels correspond to

$$\tau^{\mathrm{Au}}_{xy,\max} \cong 1.17\,(E\alpha)_{\mathrm{Au}}\ \overline{\Delta T}\ \text{(in Gold)},$$
$$\sigma^{\mathrm{Au}}_{xx,\max} \cong -1.72\,(E\alpha)_{\mathrm{Au}}\ \overline{\Delta T}\ , \qquad (11)$$
$$\alpha^{\mathrm{Au}}_{zz,\max} \cong 1.3\,(E\alpha)_{\mathrm{Au}}\ \overline{\Delta T}\ ,$$

where $\overline{\Delta T}$ is the mean temperature rise in the gold absorber, $(\alpha E)_{\mathrm{Au}}$ being evaluated for gold. For the compressive stress in the silicon the maximum stress level is

$$\sigma^{\mathrm{Si}}_{xx,\max} \cong -9.63(E\alpha)_{\mathrm{Si}}\ \Delta T_{\mathrm{in}}\ , \qquad (12)$$

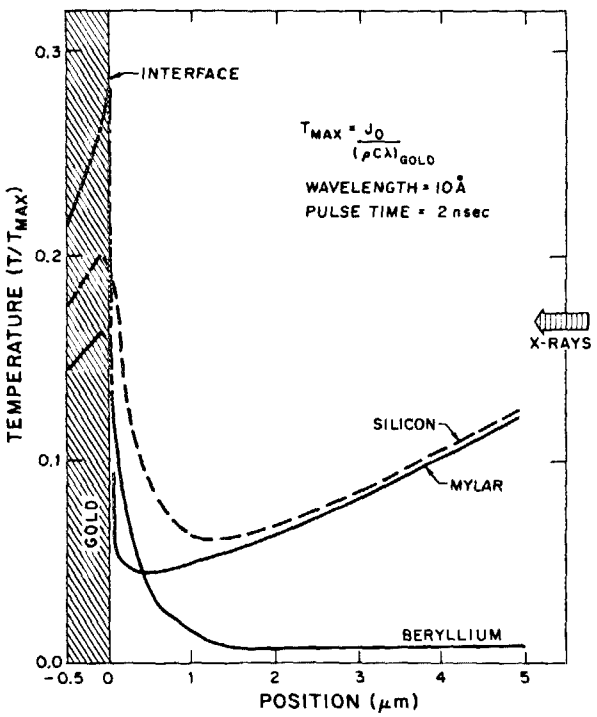

FIG. 7. Temperature profiles in various mask structures for a 2-ns x-ray pulse.

where ΔT_{in} is the interface temperature between the gold and silicon and $(\alpha E)_{\mathrm{Si}}$ being evaluated for silicon. It can be seen, therefore, that the presence of the high thermal expansion gold layer acts to induce very large compressive stresses in the silicon substrate at the ends of the absorbing block.

The code prediction of shear stress generated in the gold can be seen to be significantly smaller than that obtained from the rigid substrate model [cf. Eq. (9)] as a consequence of strain reduction through induced strain in the substrate.

In addition to computations made for the initial maximum stress levels generated at the end of the x-ray pulse, the equilibrated temperature profile (i.e., constant temperature) case was also run. The stress levels correspond to

$$\sigma^{\mathrm{Au}}_{xy,\mathrm{equil}} \cong 0.98(E\alpha)_{\mathrm{Au}}\ \Delta T_{\mathrm{equil}} \cong 0.43(E\alpha)_{\mathrm{Au}}\ \overline{\Delta T}\ ,$$
$$\sigma^{\mathrm{Au}}_{xx,\mathrm{equil}} \cong -1.41(E\alpha)_{\mathrm{Au}}\ \Delta T_{\mathrm{equil}} \cong -0.62(E\alpha)_{\mathrm{Au}}\ \overline{\Delta T}\ , \qquad (13)$$

where $\Delta T_{\mathrm{equil}}$ is the equilibrated temperature of the mask.

For the silicon the compressive stress is given by

$$\sigma^{\mathrm{Si}}_{xx,\mathrm{equil}} = -7.85(E\alpha)_{\mathrm{Si}}\ \Delta T_{\mathrm{equil}} = -3.45(E\alpha)_{\mathrm{Si}}\ \Delta T_{\mathrm{in}}\ . \qquad (14)$$

Thus, it can be seen that the very rapid heating leads to stress levels which are about 2.3 times greater than those of the thermally equilibrated mask.

3. Failure criteria

There is some doubt as to the actual magnitude of what we may call a failure stress. This has several reasons. The state of intrinsic stress is itself not characterized as well as we would like. Although much work has been done on establishing levels of stress in thin films, the detailed microstructure of the stress field has not been established. Certainly the state of the stress in a thin film may be a large fraction of the ultimate strength of the material.[18] These stresses may also vary with the specific conditions of layer formation (temperature history, layer thickness, residual gas/impurity levels).[18,19] For gold films (about 1000 Å thick), upon quartz and copper substrates, (references in Chopra[18]), tensile stresses of about 4200 and about 12 000 psi have been measured. The interpretation of the stress field is therefore complicated by the presence of intrinsic stress levels. For the purposes of the modeling carried out here, we have taken the initial stress state to be zero. This has the effect of giving a factor-of-2 uncertainty in the failure temperature of fluence; i.e., the stress being cycled from $+\sigma_{\mathrm{ult}}$ to $> -\sigma_{\mathrm{ult}}$.

The mechanism of failure may take several forms, depending upon the definition of failure. Failure may be a catastrophic delamination of the absorber from the substrate, a stress failure of the substrate, or an inability to obtain the desired level of resolution of the lithographic process as a consequence of plastic strain in the mask structure. This failure may occur as a consequence of a single-pulse irradiation, or, more importantly, over a large number of pulses by a fatigue failure.

Delamination of the absorbing layer occurs if the stress exceeds the adhesion strength of the interface region. There is evidence that is can be very high. For example, Benjamin

and Weaver[20] mesured adhesive stresses of some 5000–12 000 psi for gold on salt crystals. Conversely, Nenadovic *et al.*[21] only obtained values of 150–750 psi on acrylate and glass substrates (film thickness $<0.15\,\mu$m). For want of better data we have taken a single-pulse damage criterion as being equivalent to the yield stress of the gold material. This varies from 7000 to 28 000 psi.[22,23] The ultimate strength of 0.5-μm-thick gold is in the range of 40 000–45 000 psi.[24]

On a fatigue basis, either delamination or cracking of the substrate is possible. The stress level below which fatigue will not occur is known as the endurance stress σ_e.[25] For nonferrous materials, one can expect $\sigma_e \sim 0.25\,\sigma_{\text{ult}}$. We are likely to be in a regime in which the total lifetime pulse requirement for a mask may be of order 10^6 pulses.

For nonzero initial or mean stress, the effective stress may be expressed in terms of stress components.[26]

$$\sigma_e \sim (\sigma^2_{xx,\max} - \sigma_{xx,\max}\,\sigma_{zz,\max} + \sigma^2_{zz,\max} + 3\,\tau^2_{xz,\max})^{1/2} - \left(1 - \frac{\sigma_a}{\sigma_{\text{yield}}}\right)(\sigma^2_{xx,\text{mean}} - \sigma_{xx,\text{mean}}\,\sigma_{zz,\text{mean}} + \sigma^2_{zz} + 3\,\tau^2_{xz,\text{mean}})^{1/2}. \quad (15)$$

The generation of fatigue failure will be a function of the pattern of cyclic loading. In general, cyclic loading is assumed to be sinusoidal. We do not have such behavior, but rather a series of quasi square pulses at intervals very much greater than their duration. This makes it difficult to assess the required magnitude of the stress to cause failure. However, on the basis of a mean stress that is effectively zero, this yields from Eqs. (11) and (15)

$$\sigma_e \sim 2.5(E\alpha)_{\text{Au}}\,\overline{\Delta T}\,. \quad (16)$$

Taking $\sigma_e \sim 10\,000$–$12\,000$ psi yields a maximum allowable temperature rise of $\sim$26–31 K, or in terms of a resist dosage, 5–6 mJ/cm^2/pulse.

If we assume only an intrinsic compressive stress, of magnitude σ_{yield}, we obtain

$$\sigma_e \sim 2.5(E\alpha)_{\text{Au}}\,\overline{\Delta T} - 0.5\sigma_y\,, \quad (17)$$

thereby increasing the maximum dosage to approximately 7–8.5 mJ/cm^2 for $\sigma_y = 8000$ psi. However, at this time the state of knowledge of the fatigue or delamination failure of such structures is at best limited, so the failure criterion for the gold will be taken as that corresponding to Eq. (16).

For the substrate the dominant stress is the axial compressive one. Taking an ultimate strength of the substrate as about 60 000 psi,[28] yields a fatigue limit of approximately 7 mJ/cm^2 pulse, which is comparable with the gold.

To summarize, the level of stress necessary to do damage to the mask has been taken as that corresponding to the endurance limit of the material for fatigue. Failure may arise out of a delamination of the gold absorber from the substrate, or a cracking and bulk damage of the mask. The bounds upon thermal loading are subject to uncertainties with respect to intrinsic stress levels and also to adhesive or bonding strength. The present evaluation for a gold/silicon mask is a maximum pulse fluence of 5–6 mJ/cm^2/pulse at the resist, or about 14–17 mJ/cm^2/pulse incident on the mask.

4. Intermediate interface materials

One aspect of the present mask design is that of providing adequate bonding between mask substrate and absorber by means of an intermediate layer. Thus, gold/silicon masks usually have a thin layer of chromium ($\sim$200 Å) between absorber and substrate. Tantalum has also been used as an intermediate. The question arises as to the influence of such intermediate layers upon stress levels and the prospect of suitably choosing such materials to modify the stress levels.

The use of chromium and tantalum as intermediate materials has been found to not significantly alter the shear stress levels generated at the interface of a gold/silicon mask, as the whole mask is effectively clamped for the relevant time scale. However, as a consequence of such a clamping of the substrate material, the compressive stress generated in the intermediate materials can be very high. For a gold on silicon mask, at a dosage of 10 mJ/cm^2, the stress generated in the vicinity of the end of the gold absorbing block is about 20 000 psi. For a thin layer of tantalum and/or chromium the stresses are increased by 40% to 28 000 psi. Under such conditions it would be expected that considerable plastic deformation would occur in the interface region. For both of these materials the ultimate strength is of order 70 000 psi, giving a maximum allowable lifetime stress of about 17 000 psi, and a corresponding maximum allowable x-ray dosage of order 6 mJ/cm^2. Cummulative damage is likely to occur at these interface regions for fluences in excess of this level. This corresponds very closely to the limit due to delamination by shear/fatigue for the gold, which was estimated to be about 5 mJ/cm^2. As such layers are very thin, any imperfection in structure may lead to cracking and subsequent shear-initiated delamination of the gold absorber. The nature of such interface materials must therefore be considered very carefully in mask design for pulsed applications.

5. Variation of substrate material

The substrate material described up to this point has been considered to be silicon. It is a relatively well-understood material with good handling qualities. In order to investigate the potential gains of changing the substrate material we have examined, for illustrative purposes, beryllium and a plastic (Mylar). The relevant physical parameters are given in Table III. The temperature profiles existing at the end of the x-ray pulse are shown in Fig. 7. As can be seen, the beryllium, owing to its low absorption coefficient, has markedly lower temperatures than the silicon. The rationale for examining beryllium is partly on these grounds, and also because of its close proximity to gold in terms of thermal expansion. This should, in principle, reduce the shear stress

TABLE III. Mask material properties.

Material	Young's modulus E (psi $\times 10^7$)	Expansion coefficient ($K^{-1} \times 10^6$)	Absorption depth (μm) at $\lambda = 10$ Å
Gold	1.08	14.2	0.14
Silicon	1.55	2.2	5.0
Beryllium	4.2	11.3	17.0
Mylar	8.0	17.0	4.0

levels, and this does in fact occur. The maximum shear stress is reduced by a factor of 2.1 as compared to silicon. The compressive stress at the interface is also slightly lower than for silicon ($\simeq$90%). A map of shear in the vicinity of the gold absorber is shown in Fig. 8.

The large interfacial stresses near the interface are due to induced strain by the gold absorber. This would lead us to expect that significant reduction in Young's modulus for the substrate could substantially reduce the effect of the local strain and hence the stress levels. By selecting Mylar as a substrate we can examine the consequences of this premise. Figure 9 illustrates the shear stresses for this case; as can be observed, there is a dramatic reduction in stress levels. The compressive stress is likewise reduced, being only 45% of that of silicon.

These results indicate that plastic substrate materials can be effective in reducing the compressive and shear stressed in the absorber laser.

The problems with delamination may be reduced by encapsulation. For example, Maydan *et al.*[28] used a protective covering over the gold absorber. The value of this technique is that it can significantly reduce the shear loading on the absorber. However, it we consider the absorber to be surrounded by a rigid substrate, the appropriate compressive stress level is

$$\sigma_{xx} = \frac{E\alpha T}{1-2\nu} = -6.25\,(E\alpha)_{\mathrm{Au}}\,T, \tag{18}$$

which is a factor of 2 higher than for the exposed absorber model described earlier. The use of plastic as a substrate material should reduce the stress somewhat.

IV. SUMMARY

The levels of stress generated by pulsed irradiation of several prototypical materials have been evaluated and examined in the light of both delamination of fracture by single pulse irradiation as well as that of multiple-pulse fatigue failure. The influence of thermal and mechanical properties upon these stress levels has been examined and the subsequent impact of these upon the allowable maximum dosages of x rays has been investigated. However, at this time the exact limits are subject to some uncertainty due to a lack of both data of interface properties as well as any experimental data of such intense pulsed x-ray interaction with representative structures.

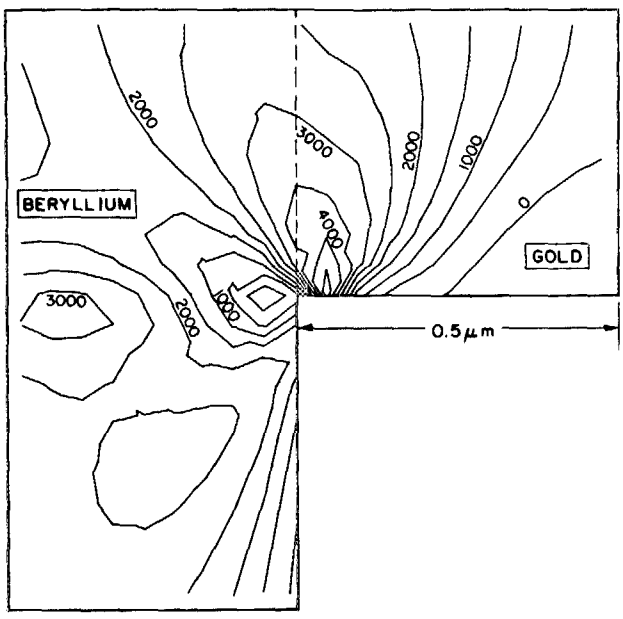

FIG. 8. Shear stress field for the interface region of a beryllium/gold mask, with $J_0 = 10$ mJ/cm^2 (stress in psi).

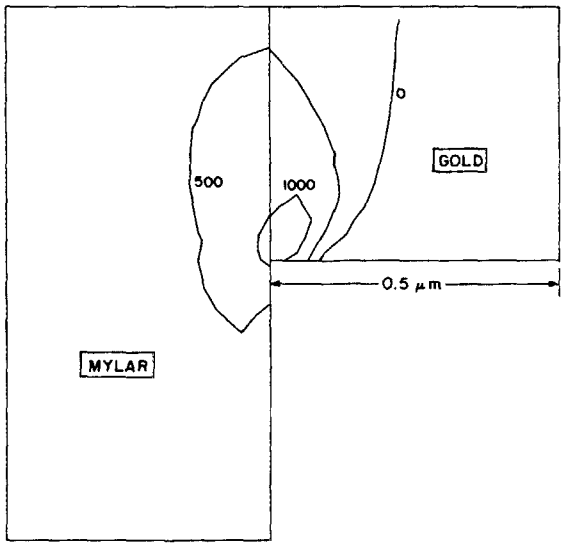

FIG. 9. Shear stress field for the interface region of a Mylar/gold mask with $J_0 = 10$ mJ/cm^2 (stress in psi).

ACKNOWLEDGMENT

We would like to acknowledge the support of the Rome Air Development Center, Air Force Systems Command under Contract No. F19628-80-C-0176.

APPENDIX A

Analytical model for absorber/substrate interface stress

We consider here a block of heated material (the absorber) mounted on a rigid layer (the substrate), as depicted in Fig. A1. This is a simplification, of course, as the substrate will deform as the heated absorber undergoes thermal expansion. Further, the block, which has in fact dimensions in the y direction approximately equal to those in the x direc-

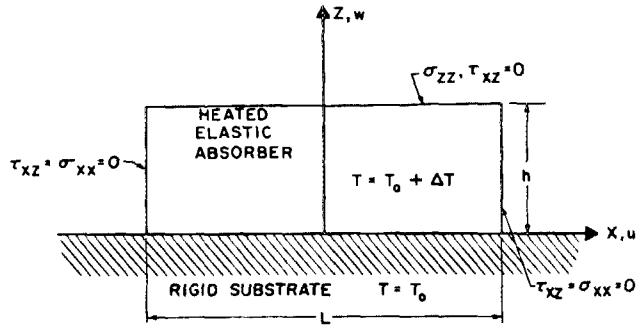

FIG. A1. Stress model geometry.

tion, is considered to be in plane-strain normal to the paper.

A simple solution is effected by assuming a displacement field in the form

$$u(x, z) = k\,(Ahz + Bz^2)\sinh(kx)\,, \tag{A1}$$

$$w(x, z) = Chz\cosh(kx)\,, \tag{A2}$$

$$k = \sqrt{\frac{1-2\nu}{2(1-\nu)}\left(\frac{\pi}{2h}\right)}\,, \tag{A3}$$

where A, B and C are, so far, arbitrary constants. Two of these constants are determined by requiring that the shear stress τ_{xz} vanish on the top of the block ($z = h$) and that an "energy" average of the transverse normal stress G_{xx} vanish there also. Thus

$$\tau_{xz}(x, h) = G\left(\frac{\partial u(x, h)}{\partial z} + \frac{\partial w(x, h)}{\partial x}\right) = 0\,, \tag{A4}$$

and

$$\int_0^{L/2} \sigma_{xx}(x, h)\cosh(kx)\,dx = \frac{E}{(1-\nu)(1+2\nu)}\int_0^{L/2}\left((1-\nu)\frac{\partial u(x, h)}{\partial x} + \frac{\partial w(x, h)}{\partial z} - (1+\nu)\alpha\Delta T\right)\cosh(kx)\,dx = 0\,. \tag{A5}$$

The enforcement of these conditions yields a pair of equations for the constants A and B, as follows:

$$A = (1-2\beta)Ch + 2\phi\,, \tag{A6}$$

$$B = (1-\beta)Ch - \phi\,. \tag{A7}$$

There β and ϕ are given by

$$\beta = \frac{1}{k^2h^2}\left(\frac{1-\nu}{\nu}\right) = \frac{8(1-\nu)^2}{\pi^2\nu(1-2\nu)}\,, \tag{A8}$$

$$\phi = \frac{4(1+\nu)\alpha\Delta T}{(kh)^2}\left(\frac{\sinh(kL/2)}{kL + \sinh(kL)}\right). \tag{A9}$$

Now, the constant C is determined by minimizing the potential energy of the block, whose strain energy density is

$$U_0 = G\left\{\left(\frac{1-\nu}{1-2\nu}\right)\left[\left(\frac{\partial u}{x}\right)^2 + \left(\frac{\partial w}{\partial z}\right)^2\right] + \left(\frac{2\nu}{1-2\nu}\right)\frac{\partial u}{\partial x}\frac{\partial w}{\partial z} + \frac{1}{2}\left(\frac{\partial u}{\partial z} + \frac{\partial w}{\partial x}\right)\right\}^2 - \frac{E\alpha\Delta T}{(1-2\nu)}\left(\frac{\partial u}{\partial x} + \frac{\partial w}{\partial z}\right). \tag{A10}$$

Note that since no constraints or loads are applied at $x = \pm L/2$, the minimization of the strain energy implies that the axial normal stress vanishes there in an "energy average" sense, as no work is done at that boundary.

That minimization process yields, after tedious algebra,

$$Ch = \phi_r\,\frac{2\beta + 3\Lambda^2(1-2\beta) - \Lambda^2(7-32\beta)/10 - 2\dfrac{1-2\nu}{\nu}\beta\phi_r(1-2\beta)}{2\beta(1-\beta) + \Lambda^2(1-7\beta+16\beta^2)/5 + \dfrac{1-2\nu}{\nu}\beta\phi_r(1-2\beta)}\,, \tag{A11}$$

where

$$\phi_r = \frac{\sinh(kL) - kL}{\sinh(kL) + kL} \tag{A12}$$

and

$$\Lambda = \frac{1-\nu}{\nu}\,. \tag{A13}$$

It is now a straightforward excercise to obtain expressions for the stress field by combining Eqs. (A1), (A2), (A4), and (A5), and Eqs. (A6), (A7), and (A11). For a gold absorber ($\nu = 0.42$), for example, the shear stress at the interface is given by

$$\tau_{xz}(x, 0) = \frac{14.28\,E\alpha\Delta T}{1 + 1.2\phi_r}\,\frac{\sinh(kL/2)\sinh(kx)}{kL + \sinh(kL)}\,. \tag{A14}$$

[1] N. P. Economu and D. C. Flanders, J. Vac. Sci. Technol. **19**, 868 (1981).
[2] D. J. Nagel, Proc. Soc. Photo. Opt. Int. Eng. **279**, 98 (1981).
[3] H. Hyman, A. Ballantyne, H. W. Friedman, and D. A. Reilly, J. Vac. Sci. Technol. **21**, 1012 (1982).
[4] C. L. Dym and A. Ballantyne, J. Appl. Phys. **58**, 4726 (1985).
[5] D. L. Spears and H. I. Smith, Electron. Lett. **8**, 102 (1972).
[6] R. K. Watts, K. E. Bean, and T. L. Brewer, *8th International Conference on Electron and Ion Beam Science and Tech*, Seattle, Washington (Electrochemical Society, Princeton, NJ, 1978).
[7] E. Bassous, R. Feder, E. Spiller, and Topalian, Solid State Technol. **19**, 9 (1976).
[8] P. A. Sullivan, and J. H. McCoy, IEEE Trans. Electron Devices **ED-23**, 412 (1976).
[9] P. Parrens, E. Tabouset, and M. C. Tacussel, J. Vac. Sci. Technol. **16**, 1965 (1979); D. Hofer, J. Powers, and W. D. Grobman, J. Vac. Sci. Technol. **16**, 1968 (1979).
[10] D. Maydan, G. A. Coquin, J. R. Maldonado, S. Somek, D. Y. Lou, and G. N. Taylor, IEEE Trans. Electron Devices **ED-22**, 429 (1975).
[11] D. J. Nagel, M. C. Pekerar, R. R. Whittock, J. R. Grieg, and R. E. Pechacek, Electron. Lett. **14**, 781 (1978).
[12] D. Maydan, G. A. Coquin, H. J. Levinstein, A. K. Sinha, and D. N. K. Wang, J. Vac. Sci. Technol. **16**, 1959 (1979).
[13] T. Hayashi, 8th International Conference on Electron and Ion Beam Science and Technology, Seattle, Washington (1978) (unpublished).
[14] L. Csepregi and A. J. Heuberger, J. Vac. Sci. Technol. **16**, 1962 (1979).
[15] H. S. Carslaw and J. C. Jaeger, *Conduction of Heat in Solids* (Clarendon, Oxford, 1959).
[16] W. D. Grobman, "Synchrotron Radiation X-Ray Lithography," IBM Research Report RC8220 (#35136) (11307 Research Center, Yorktown Heights, New York) (February 1980).
[17] SAFE-12 Code, based upon SAAS Code; see, for example, J. G. Crose, "Stress Analysis of Axisymmetric Solids with Asymmetric Properties," Report No. APP-72 (S2816-15)-1, The Aerospace Corporation, San Bernardino, CA (1971); J. G. Crose, and R. M. Jones, "SAAS 111 Finite Element Stress Analysis of Axisymmetric and Plane Solids with Different Orthotropic Temperature-Dependent Material Properties in Tension and Compression," Rept. No. TR-0059 (S6816-53)-1, The Aerospace Corporation, San Bernadino, CA (1971).
[18] K. L. Chopra, *Thin Film Phenomena* (McGraw-Hill, New York, 1969).
[19] J. Angilello, J. Baglin, F. d'Heurle, S. Peterson, and A. Segmuller, "Stresses in Silicides Formed by the Interaction of Metal Films with Silicon Substrates," *Proceedings of the 1977 Symposium on Thin Film Interfaces and Interactions* (Electrochemical Society, Princeton, NJ, 1977).
[20] P. Benjamin and C. Weaver, Proc. R. Soc. (London) Ser. A **274**, 267 (1963).

[21]T. Nenadovic, N. Bibic, N. Kraljevic, and M. Adamov, Thin Solid Films **34**, 211 (1976).
[22]J. W. Menter, and D. W. Pashley, *Structure and Properties of Thin Films* (Wiley, New York, 1959), p. 111.
[23]J. W. Beams, *Structure and Properties of Thin Films* (Wiley, New York, 1959), p. 183.
[24]C. A. Neugebauer, "Structural Disorder Phenomena in Thin Films," *Physics of Thin Films, Vol. 2*, edited by G. F. Hass, and R. E. Thun (Academic, New York, 1964).
[25]S. H. Crandall, N. C. Dahl, and T. J. Lardner, *An Introduction to the Mechanics of Solids* (McGraw-Hill, New York, 1978).
[26]J. H. Faupel, *Engineering Design* (Wiley, New York, 1964).
[27]W. R. Runyan, *Silicon Semiconductor Technology* (McGraw-Hill, New York, 1965).
[28]D. Maydan, E. A. Coguin, H. J. Levinstein, A. K. Sinha, and D. N. K. Wang, J. Vac. Sci. Technol. **16**, 1959 (1979).